Regenerative Therapy 26 (2024) 170–179

Contents lists available at ScienceDirect

Regenerative Therapy

journal homepage: http://www.elsevier.com/locate/reth

Original Article

Design and development of pH-responsive levofloxacin-loaded metal-organic framework for the promising treatment of pediatric abdominal wound repair

Guoyan Wang [a], Hongwei Li [a], Xinhua Shao [a], Shuisheng Teng [a], Qiong Wu [b, *]

[a] Department of Pediatric General Surgery, The First People's Hospital of Chengzhou, Chenzhou, 423000, China
[b] Department of Pediatric Respiratory Medicine, The First People's Hospital of Chengzhou, Chenzhou, 423000, China

ARTICLE INFO

Article history:
Received 25 March 2024
Received in revised form
24 April 2024
Accepted 9 May 2024

Keywords:
Levofloxacin
Metal-organic framework
Cytocompatibility
Wound scratch
Antibacterial

ABSTRACT

With over 9 million fatalities per year expected by 2030, infectious diseases will remain a significant burden on the world economy and cause high mortality rates. An excellent method to increase the bioactivity of levofloxacin (LEV) in pediatric abdominal wound repair is the finding of a stimuli-based drug delivery system (DDS). We designed and developed an LEV incorporated with zeolite imidazole framework-8 (ZIF-8) as a promising nanocarrier for wound healing applications. The spectral analysis and morphological analysis confirm the formation of our newly fabricated composites. Mouse embryonic fibroblast NIH3T3 cells, the cytotoxicity, cytocompatibility, and cell proliferation characteristics of LEV@ZIF-8 were evaluated in vitro. LEV@ZIF-8 composite considerably improved the biocompatibility against NIH3T3 cells after 72-h of exposure, according to in vitro experiments. Under acidic circumstances, the pH-responsive drug release studies exhibit superior LEV release, and in physiological circumstances, there is no unintended drug release. The LEV@ZIF-8 composite-treated cells demonstrate the most remarkable cell growth and migration method in a very short time, according to the results of the wound scratch experiment. The composite exposure concentration depended on inhibition against various microorganisms in the antibacterial activity testing. According to the study, LEV@ZIF-8 are appropriate and effective DDS for stimuli-based pediatric abdominal wound repair.

1. Introduction

0.25% and 3% of people experience dehiscence after a laparotomy, which can be attributed to various factors. Infection, hematoma, and seroma are the most prevalent local variables linked to wound breakdown [1]. Systemic factors usually combined with abdominal wound dehiscence include older age, poor nutrition, lung problems, kidney failure, fatness, chemotherapy, administration of radiotherapy, steroid use, and diabetes mellitus [2]. Regional factors include bowel oedema and abdominal distention, which intra-abdominal infections, bleeding, and trauma may cause. Wound dehiscence is also more likely to occur following rushed or botched surgeries, such as emergency laparotomies [3]. A post-laparotomy lesion can decrease superficially and locally to entirely and radically. Fascial dehiscence almost always results from a multi-bacteria illness [4]. The primary focus of therapy is to restore the abdominal wall's integrity, which can only be done by fixing the root cause of the dehiscence and creating a healthy environment for the wound to recover [5–8].

Many attempts have been made to improve the recovery of chronic lesions by employing various methods, such as growth factor, gene delivery, and cell treatment [9]. The half-life of drugs and genes can be increased, bioavailability increased, pharmacokinetics optimized, and dosage frequency reduced with the help of drug delivery devices operating at the nano, micro, and macro sizes, respectively [10]. Delivering therapeutic proteins and nucleic acids to their intracellular destinations would require a nanoparticle-mediated transport system [11]. Conversely, if only extracellular delivery is necessary, the slower release rates afforded by microparticle-mediated transport may provide a more stable therapeutic impact. Alternatively, microcapsules or microgels could transport cells [12]. The ability of tissue-engineered scaffolds to act

* Corresponding author. NO.102, Luojiajing, Chenzhou, 423000, China.
E-mail address: Qiongwu545@outlook.com (Q. Wu).
Peer review under responsibility of the Japanese Society for Regenerative Medicine.

https://doi.org/10.1016/j.reth.2024.05.003

as a depot for integrating drugs makes them attractive drug transport devices for wound healing. In addition, they can serve as actual tangible barriers between the incision and the environment. So, scaffolds that contain drugs hold great promise for mutually speeding up the mending process of chronic wounds [13].

Crystalline porous coordination polymer materials termed metal-organic frameworks (MOFs) are made from organic compounds and metallic metal ions [14]. More active sites, higher specific surface areas, higher porosity, lower skeleton density, consistent pore sizes that can be adjusted, superior temperature stability, and easy functionalization are just a few of the appealing features of MOFs [15–18]. MOFs have been extensively applied in various fields, including gas adsorption and separation, energy storage, luminescence, catalysis, detection, and proton propagation [19]. Drug delivery, biocatalysts, biosensors, and biological imaging are all areas where significant effort has been put into producing MOFs because of their adaptability based on the interplay between various metal nodes and organic connections [20].

The healing process of a lesion is highly vulnerable to bacterial infection, which can cause extensive tissue harm and even death [21]. The advent of antibacterial strategies has made wound recovery easier in recent years [22]. Various applications have been found for metal ion-releasing MOF materials, including releasing bactericidal metal ions, loading various small molecular drugs for wound chemotherapy, generating large amounts of reactive oxygen species (ROS), and heating for photodynamic or photothermal sterilization [23–25]. Nanocarbons produced from metal-organic frameworks (MOFs) have safe and effective cutaneous lesion disinfection and are immediately helpful as biocatalysts or drug carriers for accelerating wound healing [26].

Zn^{2+} is an astringent, moisturizer, and antibacterial in skincare due to its harmless antimicrobial action [26]. Antibacterial action against a wide variety of bacteria has been observed in tests of ZIF-8 (zeolite imidazolate framework material). These ZIF-8 molecules are tetrahedral in shape and contain zinc metal atoms connected by strands of imidazole units. Experiments have shown that copper and zinc ions, at exact ratios, promote cell movement, angiogenesis, collagen deposition, fibroblast migration, and proliferation, all essential for wound repair [27]. ZIF-8's antibacterial and wound healing characteristics have been confirmed, but its hydrophobic behaviour and aggregation present challenges for dispersing MOFs in hydrophilic materials, lowering its tensile strength [28]. As a result, MOFs' functional design has become an essential tactic for their widespread use in hydrogels [29]. Combining MOFs with other tissue healing strategies will help create a multifunctional skin histocompatibility substance for treating wound infection [30].

Levofloxacin's anti-inflammatory properties, rather than its antibiotic folks, have recently garnered much scholarly interest [31]. Psoriasis, hidradenitis, and folliculitis are all treated with this drug as part of a systemic immunosuppressive regimen. The amounts of inflammatory cytokines in lesions that don't heal are significantly more significant [32]. They promote the production of enzymes like proteases and lipases, which impede the wound-healing process in several ways (e.g., by degrading growth factors, stopping cell multiplication and motility, and breaking down the extracellular matrix) [33–35]. Several in vivo investigations have shown that wound recovery is boosted when levofloxacin is present. In addition, levofloxacin-induced pregnane X receptor stimulation has been linked to accelerated wound healing. In addition, the drug was effectively used for oral therapy of diabetic foot osteomyelitis [36]. Levofloxacin incorporated ZIF-8-based nanoparticles for abdominal surgery after wound healing, which was the present study's primary topic. Fabricated nano DDS will comprehensively evaluate their physicochemical characteristics using various spectral and microscopic methods [37]. In recent years, it has been used as an innovative and versatile substance for wound treatment after surgical procedures for pediatric abdominal surgery [38–40].

2. Experimental section

2.1. Materials and reagents

2-methyl imidazole, zinc nitrate hexahydrate, and levofloxacin were bought from Shanghai GL Biochem Co. Ltd. Nutrient Broth and Nutrient Agar was purchased from Beijing ZhongShuo Pharmaceutical Technology Development Co., Ltd.3-(4,5-dimethylthiazol-2-yl)-2,5-diphenyl tetrazolium bromide (MTT, Beyotime Biotechnology Co. Ltd.), acridine orange (AO). All the organic solvents were purchased from Sinopharm Chemical Reagent Co., Ltd. (Shanghai, China). Mouse embryonic fibroblast non-cancerous cells (NIH3T3) were acquired from the China Center for Type Culture Collection (CCTCC) and preserved in RPMI-1640 medium supplemented with 10% heat-inactivated fetal bovine serum, 1% penicillin-streptomycin. The cells were incubated under standard culture conditions (5% CO_2, 37 °C).

2.2. Fabrication of levofloxacin (LEV)-encapsulated ZIF-8 composite (LEV@ZIF-8)

According to earlier reports, a multifunctional LEV@ZIF-8 composite was constructed [41]. At first, Milli-Q water (50 mL) and zinc nitrate (200 mg) were mixed in a 200 mL glass container. Under magnetic stirring, 2-methyl imidazole (400 mg) and levofloxacin (20 mg) were suspended in 20 mL of methanol in a second 200 mL glass container. With magnetic stirring going at 300 revolutions per minute, the imidazole and levofloxacin solution was introduced to the zinc solutions. The construction of the LEV@ZIF-8 composite DDS was observed through a shift in colour from clear to pale golden colloid. At 14,000 rpm for 20 min, the dispersion was spun. Methanol and water (1:3) were combined three times to remove any remaining unreacted precursor molecules or contaminants. The hydrated nano colloid was desiccated using a heated air furnace set to 60 °C. for 6-h. The pure ZIF-8 was constructed using the same technique but without levofloxacin.

2.3. Assessment of drug loading efficiency

Using a straightforward decomposition technique [42], we can estimate the total levofloxacin loading into ZIF-8 frameworks. A composite of LEV@ZIF-8 containing 50 mg was dried and dissolved in 1 mL of HCl before being reduced to 15 mL with ethanol. The standard calibration curve was then used to analyze the solution's UV–visible spectrum at 278 nm. Following is the equation that was used to determine the overall quantity of drug loading:

$$\text{DL}\ (\%) = \text{Amount of drugs/Amount of drugs loaded in composites} \times 100.$$

2.4. Characterizations of LEV@ZIF-8 composite

The FTIR spectra of the various nanoparticle samples were obtained using Nicolet 6700 FTIR Spectrometer (ThermoFisher, Waltham, MA). Samples were synthesized and then lyophilized to obtain dry samples. The samples were mixed into a KBr pellet at 0.2 wt%. TEM images were acquired with an FEI Tecnai F20 TEM (Hillsboro, OR) operating at 200 kV. Rings in the reciprocal space resulting from the electron beam diffraction were analyzed using ImageJ software. The average size and zeta potential of polymersomes were determined by a Zetasizer Nano-ZS (Malvern

Instruments) at 25 °C based on dynamic light scattering (DLS) technique and electrophoresis, respectively. The LEV loading content was determined by UV–Vis spectroscopy (UH5300, Hitachi). MTT assays were calculated by measuring the absorbance at 570 nm using a microplate reader (Thermo Multiskan FC).

2.5. Drug release analyses

In vitro drug release was used to investigate the pH-response drug-release behaviour of the LEV@ZIF-8 composite. Thirty experiments were conducted using Tween 20 (0.5%) and PBS with acidic and normal conditions. Firstly, 1 mg of LEV@ZIF-8 composite was dispersed in 20 mL of Tween 20 solution and PBS (pH 5.0, 6.0, 6.5, and 7.4) with magnetic stirring (200 rpm) for the drug release experiments. Each time the mother solution was changed out for PBS, 2 mL was removed. We could determine the overall quantity of levofloxacin release by using a UV–Vis spectroscope at a wavelength of 276 nm and a normal calibration slope [43].

2.6. In vitro cytotoxicity assay

Using an MTT cell viability test, we analyzed the cytotoxic impact of the LEV@ZIF-8 composite on NIH3T3 fibroblast cells. Following a 24-h incubation period in RPMI-1640 media containing 1% FBS, NIH3T3 cells were dispersed into 96-well plates and permitted to adhere to the bottoms of the dishes. The LEV@ZIF-8 composite was dispersed in dimethyl sulfoxide (DMSO) and added to cell-containing growth media at 25–100 μM. The cells were permitted to incubate for 48-h at 37 °C with CO_2 after being treated with composite. The wells were then re-incubated for 3-h after adding 20 μL of MTT and PBS solution 48-h after the last exposure. Using a standard wavelength of 650 nm, we measured the absorption of composite cell media at 570 nm [44].

2.7. Fluorescence dead and live staining by in vitro

After seeding NIH3T3 fibroblast cells at a density of (5×10^4 cells/well) in RPMI-1640 solution, the cells were grown for 24-h. LEV@ZIF-8 composite at 100 μM was used to treat the cells after they had been incubated. A saline solution was used as a reference to treat the cells. Composite preincubation of cells for 2-h was followed by fluorescence microscopy analysis of bio targeting. Cells were stained with 0.5 mL of AO for 15 min after exposure to LEV@ZIF-8 and then rinsed with PBS to remove any remaining stain. We observed treated cells' toxicity and morphological changes using a fluorescent microscope and captured the images [45].

2.8. Wound scratch assay by in vitro

An in vitro wound scratch test was used to analyze the cell growth and migrations of scraped NIH3T3 cells. NIH3T3 cells were grown in RPMI-1640 supplemented with 10% fetal bovine serum and 1% streptomycin. After 24-h of growth at 37 °C, a clean 200 μL micro tip was used to scratch the surface of the cells in a 12-well culture dish. After scraping the lesion, we measured cell proliferation and movement at various times. Inverted phase contrast and fluorescence microscopy were used to watch and photograph the cell movement and regeneration. We measured initial injury and cell movement in the scratched region using Image J at 24-, 48-, and 72-h. We measured the overall quantity of cell migration three times to ensure accuracy [36].

2.9. Antibacterial activity by in vitro

The well diffusion technique was used to test the LEV@ZIF-8 composite's antimicrobial performance [46]. 15 We sub-cultured four human-infectious bacteria on nutritional agar. Each dish had wells drilled into it using a 1 mL micropoint. Wells of sterilized agar nutritional medium were filled with varying concentrations of LEV@ZIF-8 composite. After that, the bacterial types were inoculated, and the surface wetness was removed by air drying. Each well in a set of Petri plates has an identical layer of agar medium. Two types of *Staphylococcus aureus (S. aureus), Escherichia coli (E. coli), Pseudomonas aeruginosa (P. aeruginosa), and Staphylococcus epidermidis (S. epidermidis)*. Petri dishes were coated with composite and then kept at 37 °C for a whole day. An estimate of the bacterial zone of suppression was made, revealing the possible growth-inhibiting effects of the composite. Triplicate measurements of each bacterium were used to determine their typical zone of inhibition diameters.

2.10. Statistical analysis

All data presented are Mean ± SD. Statistical analysis was performed using Student's t-test. The differences between experimental and control groups were considered statistically significant for P value < 0.05.

3. Results and discussions

3.1. Fabrication of LEV@ZIF-8 composite

One-pot synthesis was used to construct a biocompatible DDS sensitive to external cues. 2-Methylimidazole and Zn^{2+} developed a ZIF through metal-organic bonding [47]. The simultaneous stirring technique was then employed to incorporate levofloxacin within the highly porous ZIF-8 drug containers. When given, the LEV@ZIF-8 composite guarantees drug transport at an acidic pH without breaking down under physiological circumstances. High-antibacterial-potential fibroblast cells proliferate more thanks to clever drug release in response to stimulation. The levofloxacin released at wound sites rises progressively as ZIF-8 frames degrade in acidic environments. We have developed unique antibiotic-encapsulated ZIF-8 nanoframeworks to facilitate safe wound healing.

3.2. Characterization of composites

Using powder XRD, we investigated the crystalline structure of the LEV@ZIF-8. In Fig. 1A, you can see the PXRD patterns for ZIF-8 and LEV@ZIF-8. The powder X-ray diffraction results proved the formation of LEV@ZIF-8 composite, which revealed uniform crystallinity between ZIF-8 and levofloxacin encapsulated ZIF-8 composite. The 2θ values are located at the diffraction maxima at approximately 10.39, 12.57, 14.36, 16.28, 18.47, 27.25, 29.62, and 30.47 for crystal surfaces (201), (212), (221), (311), (223), (201), (201), and (105). After levofloxacin was incorporated into the ZIF-8 structures, the XRD diffraction patterns changed, proving that the LEV@ZIF-8 composite contained levofloxacin. ZIF-8 crystal structures without levofloxacin encapsulation reveal the same crystal surfaces and 2θ values, confirming that the levofloxacin molecules were uniformly encapsulated. As a result of the levofloxacin modification, the crystal morphology of LEV@ZIF-8 was somewhat obscured by the amorphous nanoparticle surface, and the strength of the diffraction peaks was decreased. In addition, FTIR spectroscopy was used to examine levofloxacin and encapsulated functional groups of LEV@ZIF-8 composites (Fig. 1B). Peaks at 3433 cm^{-1} and

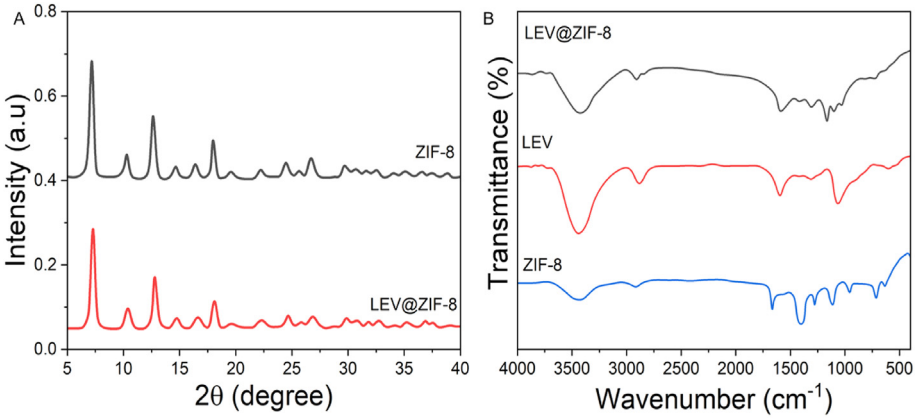

Fig. 1. Morphological characterization of composites. A) X-ray powder diffraction (XRD) spectral analysis of ZIF-8, levofloxacin (LEV), and LEV@ZIF-8 composites. B) Fourier-transform infrared spectroscopy (FTIR) spectral analysis of ZIF-8 and LEV@ZIF-8 composites.

2919 cm^{-1} indicate OH bending and CH stretching vibrations, respectively. The compound LEV@ZIF-8 shows clear peaks at 1623 cm^{-1} and 1205 cm^{-1} due to C–O and C–O–C stretching vibrations, suggesting that levofloxacin has been successfully encapsulated. When comparing the spectra of the LEV and LEV@ZIF-8 composite, we see that the distinctive peak of levofloxacin at 1062 cm^{-1} is absent in the latter, confirming the integration of levofloxacin into ZIF-8 frames. Imidazole, a common organic binder, and levofloxacin, a common antioxidant, contain benzene groups that can be stacked onto ZIF-8 [41].

UV–vis spectroscopy examined ZIF-8 and levofloxacin absorption spectra (Fig. 2A). levofloxacin, ZIF-8, and LEV@ZIF-8 all have absorbance maxima at 220, 285, and 278 nm. The homogeneous encapsulation of levofloxacin was demonstrated by a decrease in the absorption peak at 278 nm across samples of LEV@ZIF-8 composite, showing that the levofloxacin absorption site was shifted. A thermogravimetric investigation was carried out to investigate the composite's thermal stability. TGA spectra for ZIF-8, ZIF-8, levofloxacin and LEV@ZIF-8 composites are displayed in Fig. 2B. The mass loss percentage at temperature comparisons verified the thermal durability of ZIF-8 and LEV@ZIF-8 (°C). These are the two main weight loss episodes depicted by levofloxacin. The initial mass loss between 50 and 120 °C is due to water molecules released from levofloxacin. The decomposition of organic molecules from levofloxacin was verified by a second steady weight loss of 70%–85%. The breakdown of physisorbed water molecules accounts for the modest weight loss of 7% in ZIF-8 from 100 °C to 180 °C. At temperatures up to 500 °C, neither pure ZIF-8 nor the LEV@ZIF-8 composites experience appreciable mass loss [48]. Water molecules desorption on the composite's exterior surface and the breakdown of organic molecules cause the initial 13% weight loss in LEV@ZIF-8. Sharp weight loss of 65%–85% emerged after 600 °C in ZIF-8 and LEV@ZIF-8 composites. When metal and organic cooperation breaks down, it causes ZIF-8 structures to disassemble, as seen by this massive weight loss. Compared to ZIF-8, levofloxacin has greater thermal stability, suggesting that the synthesized composite is more stable and appropriate for biomedical uses.

Field emission scanning electron microscopy (FE-SEM) and transmission electron microscopy (TEM) were used to examine the morphology of the nano DDS surface after fabrication (Fig. 3). The two-dimensional flakes-like crystal shape of ZIF-8 was visible in the FE-SEM image of the pure compound. Here, the levofloxacin-incorporated LEV@ZIF-8 presents a globular aggregate. ZIF-8 appears to be a two-dimensional microgranule in the TEM image (Fig. 3). However, the LEV@ZIF-8 reveals the encapsulated polygonal particles with an average diameter of 150 nm region. Crystallization and structural regularity of levofloxacin nanoparticles were disrupted during embedding with ZIF-8 frameworks (Fig. 3). The molecules of levofloxacin served as both a reduction agent and a synthesis component in the one-pot synthesis techniques. The effective encapsulation and surface adjustments of the levofloxacin molecules in ZIF-8 formation, the morphological properties and particle size of the LEV@ZIF-8 were drastically decreased, and the crystal angles (2θ) were blurry, in contrast to the clear microscopic structure of ZIF-8 and LEV@ZIF-8.

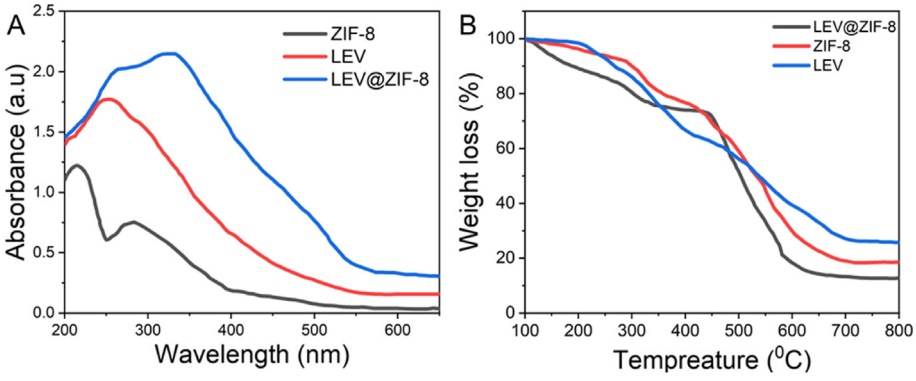

Fig. 2. A) Ultraviolet–visible (UV–vis) spectral analysis of ZIF-8, LEV, and LEV@ZIF-8 composites. B) Thermogravimetric spectral analysis of ZIF-8, LEV, and LEV@ZIF-8 composites.

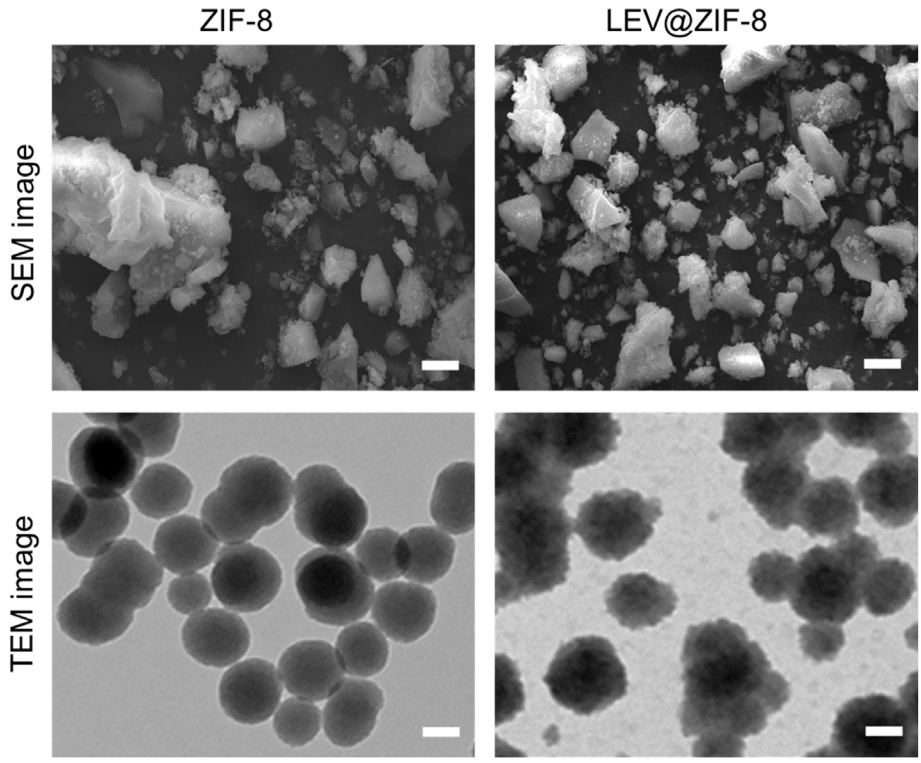

Fig. 3. Morphological characterization of composites. Scanning electron microscope (SEM) images of ZIF-8 and LEV@ZIF-8 composites. Scale bar 2 μm. Transmission electron microscopy (TEM) images of ZIF-8 and LEV@ZIF-8 composites. Scale bar 100 nm.

By utilizing DLS, we could ascertain the hydrodynamic stability of the LEV@ZIF-8 composite and the typical particle diameters of its constituents. The dynamic light scattering (DLA) analysis of a LEV@ZIF-8 composite in an aqueous medium is displayed in Fig. 4A. Composite particles, on average, are 120 ± 3.1 nm in size. The nanoparticles were consistently sized, and they dispersed very well in water. The composite's surface area and porosity were measured using the Brunel-Emmett-Teller technique. Fig. 4B shows that the LEV@ZIF-8 composite, a prime example of a microporous material, displays conventional type I N2 absorption-desorption isotherms. At 567 m^2/g, ZIF-8's BET surface area is extensive; at 152 m^2/g, LEV@ZIF-8 significantly decreases this value. Compared to raw ZIF-8, the pore volume of LEV@ZIF-8 was 0.84 cm^3/g. While ZIF-8 has microporous pores, the ones in LEV@ZIF-8 composites are mesoporous due to levofloxacin packaging, which increased the size of the metal-organic coordination interaction. The findings of the BET analysis validated the modified ZIF-8 and levofloxacin encapsulation.

3.3. Drug release property of LEV@ZIF-8 composite

The pH-mediated release was used to evaluate the efficacy of LEV@ZIF-8 composites for stimulus-responsive drug release. The LEV@ZIF-8 composites solution was to calculate the drug-loading (DL) of levofloxacin within the ZIF-8 and find a decent linear connection between the two variables. The rising tendency in levofloxacin absorbance at 278 nm with increasing quantity is depicted in Fig. 5A. Fig. 5B demonstrates that a mass ratio of 1:1 between ZIF-8 and levofloxacin results in the most remarkable loading effectiveness of the LEV@ZIF-8 composite. The total drug dosage was determined to be 41.25 ± 1.24 %. The drug-loading efficacy of the LEV@ZIF-8 composite is significantly higher than that

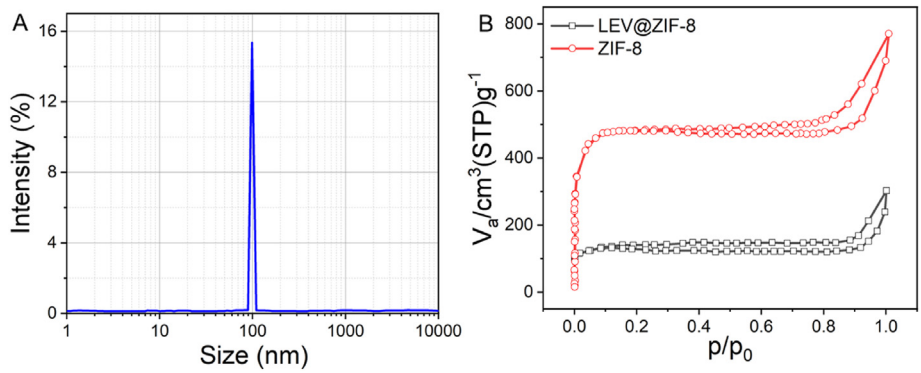

Fig. 4. A) Dynamic Light Scattering (DLS) particle size analysis of LEV@ZIF-8 composites. B) Surface area evaluation of LEV@ZIF-8 composites by BET assessment nitrogen with adsorption–desorption isotherm.

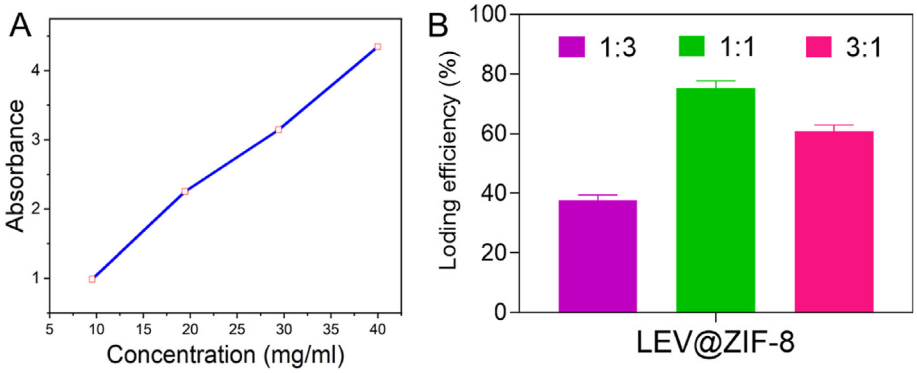

Fig. 5. A) Calibration curve of LEV at various concentrations. B) The drug-loading percentage of LEV@ZIF-8 composites at different ratios of LEV@ZIF-8 composites.

of other DDSs, and it is synthesized using a straightforward one-pot procedure. Furthermore, the pH-dependent release process of the LEV@ZIF-8 composite was measured in PBS-buffered solutions of varying pH. Fig. 6A depicts the accumulated levofloxacin release at varying pH over periods. Substantial levofloxacin release did not occur until 24-h in a physiological state, with only 10.08% of the drug being released. The ZIF-8 breaks down rapidly in acidic circumstances, leading to release. Drug release was maximized over minimal periods when the pH of PBS solutions was lowered. The ultimate assay findings revealed that drug release could be as high as 65.8% in acidic pH 5 and as low as 52.46% at pH > 6. Decomposition or fracture of MOFs bonding of ZIF-8 frameworks, as evidenced by levofloxacin release from LEV@ZIF-8 under acidic conditions. In vitro pH-mediated drug release experiments showed consistent findings. Initial dynamic data indicated that the LEV@ZIF-8 composite has excellent promise as a stimuli-responsive DDS for use in biomedicine.

3.4. Cytocompatibility of LEV@ZIF-8 composite against NIH3T3 cells

The MTT assay was used to determine if the composite of LEV@ZIF-8 had cytotoxic properties. The data showed that NIH3T3 cells were killed in a dose-dependent manner. Concentration is as high as 100 μM. After 48-h of contact, only 8% of cells had died, as shown in Fig. 6B. At 48-h, cytotoxicity is 12% in groups treated with levofloxacin alone. The biocompatibility of the compound was improved by encapsulating levofloxacin within ZIF-8 structures, which allowed for better cell death in NIH3T3 cells. The absence of damage in the control group was striking.

The live/dead cell staining technique assessed cell viability after exposure to hybrid materials. Fig. 7 demonstrates that the LEV@ZIF-8 treated groups exhibit no detectable red luminescence until 72-h after exposure. Consistently brilliant green light suggests that NIH3T3 mouse fibroblast cells are alive and well. Encapsulation, on the other hand, improves biosafety in therapeutic uses of both synthetic and natural pharmaceutics. Increased benefits in fibroblast cell safety for wound treatment after pediatric abdominal surgery will result from ZIF's excellent stability under physiological conditions.

3.5. Cell growth and wound scratch assay of LEV@ZIF-8 composite

Recovery from a wound treatment after pediatric abdominal surgery is difficult and time-consuming, often resulting in several imperfections [49]. The need for well-designed components and bacterial infections severely hampers the wound-healing process. As a result, there is an increasing need for antibacterial and innovative wound care products to help patients recover from their wounds. Avoiding microbial infection is even more crucial for effective wound recovery, making antibiotics and multipurpose materials more essential. A predetermined repair plan with stimuli-responsive key stages was necessary for wounds to recover properly. Severe inflammation prevents cells from re-epithelializing and remodelling, resulting in fibrosis. The ability of LEV@ZIF-8 composite-mediated fibroblast cells to proliferate and migrate was measured 24- to 72-h after contact. An in vitro wound scrape test reveals that the re-epithelialization stages and wound healing inflammation occur rapidly (Fig. 8). Surprisingly, our composite successfully promotes cell migration and reproduction at reduced concentrations. Fig. 7 is an inverted phase contrast micrograph of scraped NIH3T3 cells, demonstrating rapid cell growth and migration of incubation within 24-h. The live/dead test

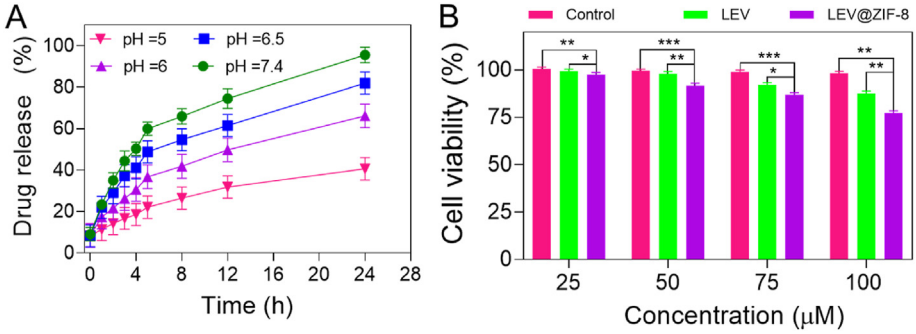

Fig. 6. A) Cumulative drug release of LEV at different pH (5.0, 6.0, 6.5, and 7.4). B) cell proliferation of LEV, LEV@ZIF-8 composites treated NIH3T3 cells in MTT assay at various concentrations (25–100 μM) for 24 (pink), 48 (green), and 72-h (violet). Data were expressed as means ± SEM (n = 3). *P < 0.05, **P < 0.01, ***P < 0.001, compared with control group.

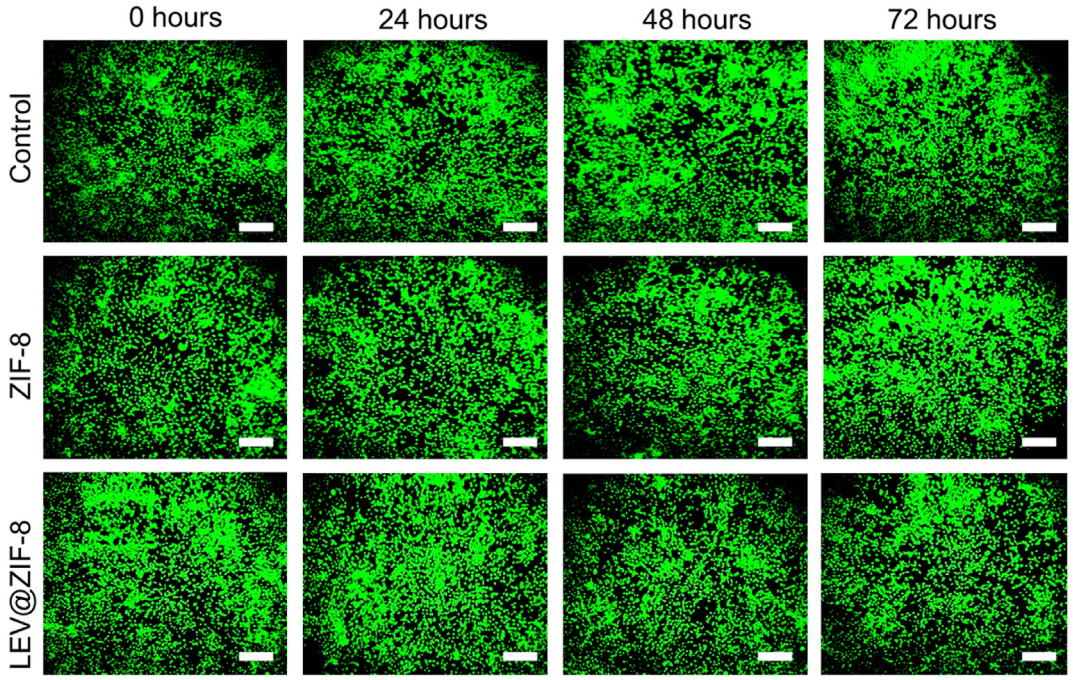

Fig. 7. For biocompatibility assessment, fluorescence microscopic images of ZIF-8 and LEV@ZIF-8 composites treated NIH3T3 cells by AO staining. Scale bar 100 μm.

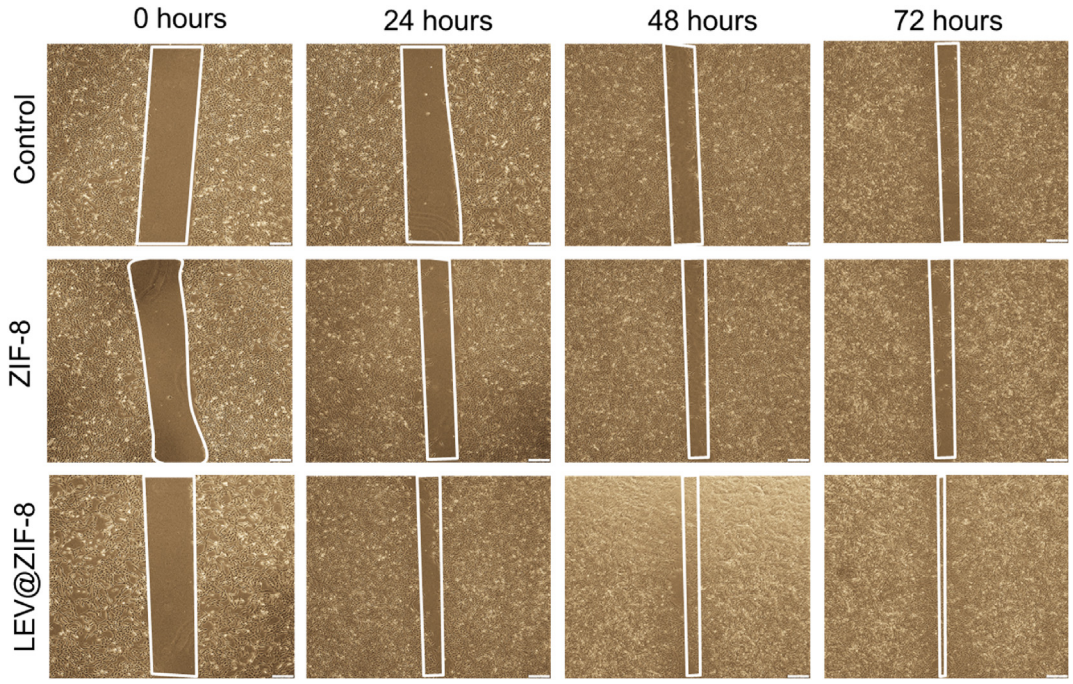

Fig. 8. Microscopic images of ZIF-8, LEV@ZIF-8 composites-treated NIH3T3 cells by wound scratch assay at different time intervals (0, 12, 24, 48, and 72 h). Scale bar 100 μm.

was also used to examine the toxicity and growth of injured cells. Within 24-h of treatment, a consistent cell migration rate can be shown in reversed fluorescence microscopy images (Fig. 8). At 24-h, the number of cells still alive and those that have multiplied in the LEV@ZIF-8 composite-treated group increased progressively. It was found that cell growth and migration were increased by a factor of four in the composite-treated groups compared to the control groups. The composite's high surface area and permeability made it an ideal environment for epidermis re-epithelialization. The microscopic findings and final in vitro scratch test results indicate that the fabricated LEV@ZIF-8 composite is a strong contender for stimuli-responsive wound treatment after pediatric abdominal surgery [50–52].

3.6. Antibacterial activity against skin pathogens

Slowing down the recovery from a laceration is a bacterial illness. Bacterial infection in wound recovery is receiving more and

more research and focus. Infectious germs colonize all post-c-section incisions and slow the healing process. Evidence of bacterial diseases within incisions harbouring biofilm communities is mounting. The germs are shielded from the host and evolve tolerance to the drugs used to treat them. The antibacterial activity of LEV@ZIF-8 against different common wound pathogens (Escherichia coli, Staphylococcus aureus, Pseudomonas aeruginosa, and Staphylococcus epidermidis) was investigated using the well diffusion technique in aerobic circumstances. Fig. 9 demonstrates that the LEV@ZIF-8 composite showed a dose-dependent increase in bacterial inhibitory activity. When composite at 75 μg/mL and 100 μg/mL, the suppression zone for treated bacteria is more significant than 17 and 19 mL. Based on these findings, levofloxacin, in addition to ZIF-8, reduces bacterial proliferation and survival. Furthermore, ZIF-8-released zinc ions can cause bacterial cell membrane impairment and subsequent cell mortality. Zinc ions' bactericidal qualities against wound bacteria are enhanced by their synergistic impact in penetrating cells and generating reactive oxygen species. LEV@ZIF-8 employs DNA topoisomerase activities and inhibits protein synthesis in bacteria to exercise its antibacterial qualities. However, when the levofloxacin concentration is high enough, the organelle of the bacterium cell is destroyed. Based on the diffusion test results, it was determined that the fabricated composite is a superior substance for eliminating wound-infecting bacteria and promoting wound healing via antibiotic action [53].

4. Conclusions

The current investigation showed that levofloxacin could be effectively encapsulated within ZIF-8 frameworks to generate pH-response LEV@ZIF-8 composites. The drug-loading capability of the synthesized composite was 40.32%. Outstanding stimuli-response drug release capability under acidic circumstances was verified by the composite's in vitro drug release. There was a significant decrease in the proliferation of Escherichia coli, Staphylococcus aureus, Pseudomonas aeruginosa, and Staphylococcus epidermidis in the presence of the composites. Synergetic impacts of levofloxacin molecules and zinc(II) ions mediated antimicrobial system were observed in the LEV@ZIF-8 composite. Analysis of LEV@ZIF-8 biocompatibility in culture showed that it was neither immunogenic nor harmful to NIH3T3 fibroblast cells. A scratch model was used to verify that the fabricated composite significantly increased the growth and movement of injured cells. The pH-sensitive drug release results determined that the synthesized composite was robust under neutral pH. The rapid levofloxacin release (65.8%) in acidic circumstances shows that the composite is

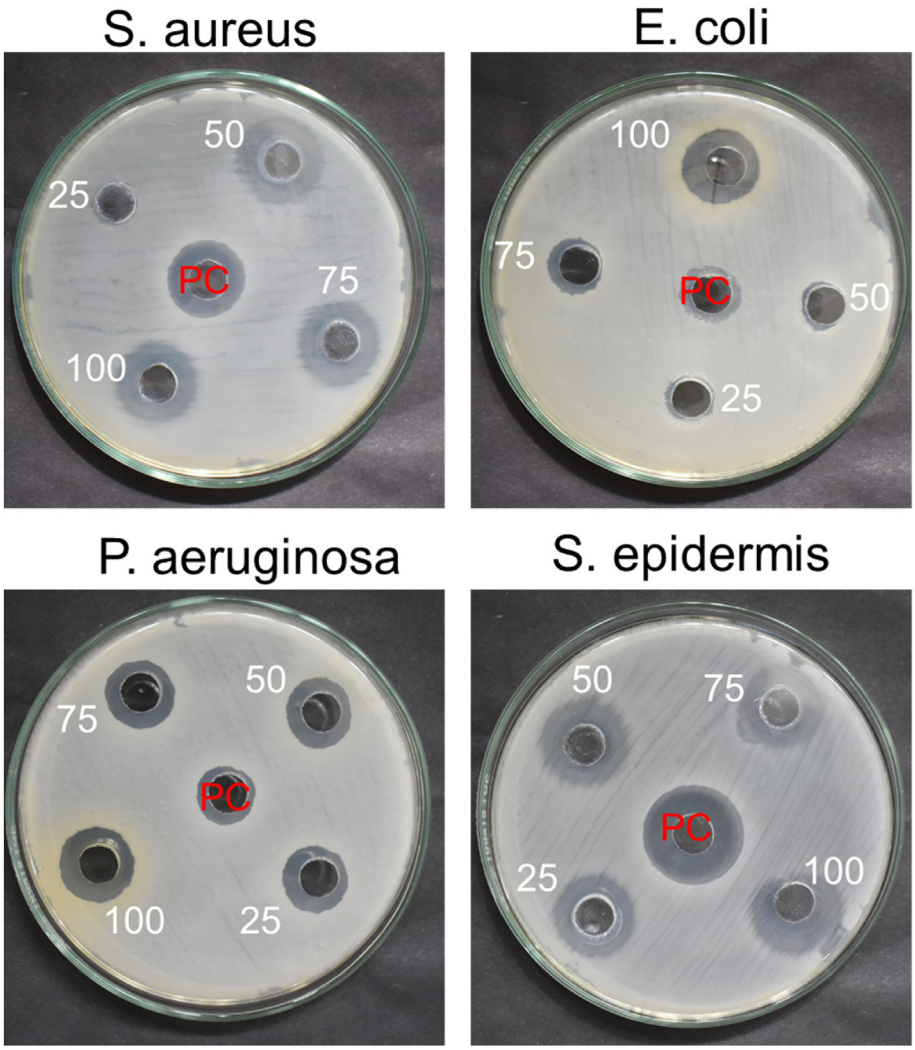

Fig. 9. The antibacterial ability of LEV@ZIF-8 composites with different concentrations of Staphylococcus *aureus (S. aureus), Escherichia coli (E. coli), Pseudomonas aeruginosa (P. aeruginosa), and Staphylococcus epidermidis (S. epidermidis)* human pathogens in well diffusion assay (zone of inhibition).

an improved option for pH-responsive drug delivery. This investigation demonstrates that LEV@ZIF-8 composites show exceptional promise as a DDS for wound treatment after pediatric abdominal surgery.

Data availability

Data will be made available on request.

Declaration of competing interest

The authors declare that they have no known competing financial interests or personal relationships that could have appeared to influence the work reported in this paper.

References

[1] Usansky I, Jaworska P, Asti L, Kenny FN, Hobbs C, Sofra V, et al. A developmental basis for the anatomical diversity of dermis in homeostasis and wound repair. J Pathol 2021;253:315–25.
[2] Losick VP, Duhaime LG. The endocycle restores tissue tension in the Drosophila abdomen post wound repair. Cell Rep 2021;37.
[3] Denys A, Monbailliu T, Allaeys M, Berrevoet F, van Ramshorst GH. Management of abdominal wound dehiscence: update of the literature and meta-analysis. Hernia 2021;25:449–62.
[4] Kane NM, Cronan JJ, Dorfman GS, DeLuca F. Pediatric abdominal trauma: evaluation by computed tomography. Pediatrics 1988;82:11–5.
[5] Liu Z, Wei N, Tang R. Functionalized strategies and mechanisms of the emerging mesh for abdominal wall repair and regeneration. ACS Biomater Sci Eng 2021;7:2064–82.
[6] Correa-Gallegos D, Rinkevich Y. Cutting into wound repair. FEBS J 2022;289:5034–48.
[7] Russello D, Sofia M, Conti P, Latteri S, Pesce A, Scaravilli F, et al. A retrospective, Italian multicenter study of complex abdominal wall defect repair with a Permacol biological mesh. Sci Rep 2020;10:3367.
[8] Villa G, Lanini I, Amass T, Bocciero V, Scirè Calabrisotto C, Chelazzi C, et al. Effects of psychological interventions on anxiety and pain in patients undergoing major elective abdominal surgery: a systematic review, Perioper. Méd 2020;9:1–8.
[9] Shariati A, Hosseini SM, Chegini Z, Seifalian A, Arabestani MR. Graphene-based materials for inhibition of wound infection and accelerating wound healing. Biomed Pharmacother 2023;158:114184.
[10] Chen T-Y, Wen T-K, Dai N-T, Hsu S. Cryogel/hydrogel biomaterials and acupuncture combined to promote diabetic skin wound healing through immunomodulation. Biomaterials 2021;269:120608. https://doi.org/10.1016/j.biomaterials.2020.120608.
[11] Liu X, Xu H, Zhang M, Yu D-G. Electrospun medicated nanofibers for wound healing. Membranes 2021;11:770.
[12] Dev A, Mohanbhai SJ, Kushwaha AC, Sood A, Sardoiwala MN, Choudhury SR, et al. κ-carrageenan-C-phycocyanin based smart injectable hydrogels for accelerated wound recovery and real-time monitoring. Acta Biomater 2020;109:121–31. https://doi.org/10.1016/j.actbio.2020.03.023.
[13] Shanmugapriya K, Palanisamy S, Boomi P, Subaskumar R, Ravikumar S, Thayumanavan T. An eco-friendly Gnaphalium polycaulon mediated silver nanoparticles: synthesis, characterization, antimicrobial, wound healing and drug release studies. J Drug Deliv Sci Technol 2021;61:102202. https://doi.org/10.1016/j.jddst.2020.102202.
[14] Cao J, Li X, Tian H. Metal-organic framework (MOF)-based drug delivery. Curr Med Chem 2020;27:5949–69.
[15] Lakshmi BA, Kim S. Current and emerging applications of nanostructured metal–organic frameworks in cancer-targeted theranostics. Mater Sci Eng C 2019;105:110091.
[16] El-Bindary AA, Toson EA, Shoueir KR, Aljohani HA, Abo-Ser MM. Metal–organic frameworks as efficient materials for drug delivery: synthesis, characterization, antioxidant, anticancer, antibacterial and molecular docking investigation. Appl Organomet Chem 2020;34:e5905.
[17] Liu J, Huang J, Zhang L, Lei J. Multifunctional metal–organic framework heterostructures for enhanced cancer therapy. Chem Soc Rev 2021;50:1188–218.
[18] Lai X, Liu H, Zheng Y, Wang Z, Chen Y. Drug loaded nanoparticles of metal-organic frameworks with high colloidal stability for anticancer application. J Biomed Nanotechnol 2019;15:1754–63.
[19] Fardjahromi MA, Nazari H, Tafti SMA, Razmjou A, Mukhopadhyay S, Warkiani ME. Metal-organic framework-based nanomaterials for bone tissue engineering and wound healing. Mater Today Chem 2022;23:100670.
[20] Wang Y, Li Q, Deng M, Chen K, Wang J. Self-assembled metal-organic frameworks nanocrystals synthesis and application for plumbagin drug delivery in acute lung injury therapy. Chin Chem Lett 2022;33:324–7.
[21] Hamed SH, Azooz EA, Al-Mulla EAJ. Nanoparticles-assisted wound healing: a review, Nano Biomed. Eng 2023;15.
[22] Maranescu B, Visa A. Applications of metal-organic frameworks as drug delivery systems. Int J Mol Sci 2022;23:4458.
[23] Yu M, You D, Zhuang J, Lin S, Dong L, Weng S, et al. Controlled release of naringin in metal-organic framework-loaded mineralized collagen coating to simultaneously enhance osseointegration and antibacterial activity. ACS Appl Mater Interfaces 2017;9:19698–705. https://doi.org/10.1021/acsami.7b05296.
[24] Moharramnejad M, Malekshah RE, Ehsani A, Gharanli S, Shahi M, Alvan SA, et al. A review of recent developments of metal–organic frameworks as combined biomedical platforms over the past decade. Adv Colloid Interface Sci 2023:102908.
[25] Mete D, Yemeztaşlıca E, Şanlı-Mohamed G. Sorafenib loaded ZIF-8 metal-organic frameworks as a multifunctional nano-carrier offers effective hepatocellular carcinoma therapy. J Drug Deliv Sci Technol 2023;82:104362.
[26] Chen Y, Cai J, Liu D, Liu S, Lei D, Zheng L, et al. Zinc-based metal organic framework with antibacterial and anti-inflammatory properties for promoting wound healing. Regen Biomater 2022;9.
[27] Ghaee A, Karimi M, Lotfi-Sarvestani M, Sadatnia B, Hoseinpour V. Preparation of hydrophilic polycaprolactone/modified ZIF-8 nanofibers as a wound dressing using hydrophilic surface modifying macromolecules. Mater Sci Eng C 2019;103:109767.
[28] Taheri M, Ashok D, Sen T, Enge TG, Verma NK, Tricoli A, et al. Stability of ZIF-8 nanopowders in bacterial culture media and its implication for antibacterial properties. Chem Eng J 2021;413:127511. https://doi.org/10.1016/j.cej.2020.127511.
[29] Yaqub A, Rashid M, Ditta SA, Malkani N, Ali NM, Yousaf MZ, et al. In vivo antioxidant potential of biogenic silver nanoparticles synthesized from Psidium guajava L. Nano Biomed Eng 2023;15:225–38.
[30] Ding Y, Yuan J, Mo F, Wu S, Ma Y, Li R, et al. A pH-responsive essential oil delivery system based on metal–organic framework (ZIF-8) for preventing fungal disease. J Agric Food Chem 2023;71:18312–22. https://doi.org/10.1021/acs.jafc.3c04299.
[31] Chen R, Xu C, Lei Y, Liu H, Zhu Y, Zhang J, et al. Facile construction of a family of supramolecular gels with good levofloxacin hydrochloride loading capacity. RSC Adv 2021;11:12641–8. https://doi.org/10.1039/D1RA00809A.
[32] Yang W, Ji X. Analysis of the microbial species, antimicrobial sensitivity and drug resistance in 2652 patients of nursing hospital. Heliyon 2020;6:e03965. https://doi.org/10.1016/j.heliyon.2020.e03965.
[33] Fathi A, Gholami M, Motasadizadeh H, Malek-Khatabi A, Sedghi R, Dinarvand R. Thermoresponsive in situ forming and self-healing double-network hydrogels as injectable dressings for silymarin/levofloxacin delivery for treatment of third-degree burn wounds. Carbohydr Polym 2024:121856.
[34] Wu L-N, Yang Y-J, Huang L-X, Zhong Y, Chen Y, Gao Y-R, et al. Levofloxacin-based carbon dots to enhance antibacterial activities and combat antibiotic resistance. Carbon NY 2022;186:452–64.
[35] Cheng Y, Chang Y, Ko Y, Liu CJ. Sustained release of levofloxacin from thermosensitive chitosan-based hydrogel for the treatment of postoperative endophthalmitis. J Biomed Mater Res Part B Appl Biomater 2020;108:8–13.
[36] Suhail Z, Shoukat H, Sanbhal N, Chowdhry N, Bhutto MA, Soomro SA, et al. Controlled drug release and antibacterial properties of levofloxacin-loaded silk/chitosan green composite for wound dressing. Biomed Mater Devices 2023;1:796–804.
[37] Koumentakou I, Terzopoulou Z, Michopoulou A, Kalafatakis I, Theodorakis K, Tzetzis D, et al. Chitosan dressings containing inorganic additives and levofloxacin as potential wound care products with enhanced hemostatic properties. Int J Biol Macromol 2020;162:693–703.
[38] Yang J, Bao C, Gu J. Investigating how tamsulosin combined with levofloxacin impacts wound healing in patients with chronic prostatitis who may also have perineal or urethral wounds. Int Wound J 2024;21:e14656.
[39] Razdan K, Kanta S, Chaudhary E, Kumari S, Rahi DK, Yadav AK, et al. Levofloxacin loaded clove oil nanoscale emulgel promotes wound healing in Pseudomonas aeruginosa biofilm infected burn wound in mice. Colloids Surf B Biointerfaces 2023;222:113113.
[40] Valizadeh A, Shirzad M, Pourmand MR, Farahmandfar M, Sereshti H, Amani A. Levofloxacin nanoemulsion gel has a powerful healing effect on infected wound in streptozotocin-induced diabetic rats. Drug Deliv Transl Res 2021;11:292–304.
[41] Ma Y, Zhao R, Shang H, Zhen S, Li L, Guo X, et al. pH-responsive ZIF-8-based metal–organic-framework nanoparticles for termite control. ACS Appl Nano Mater 2022;5:11864–75. https://doi.org/10.1021/acsanm.2c02856.
[42] Hajiashrafi S, Motakef Kazemi N. Preparation and evaluation of ZnO nanoparticles by thermal decomposition of MOF-5. Heliyon 2019;5:e02152. https://doi.org/10.1016/j.heliyon.2019.e02152.
[43] Kumar A, Wang X, Nune KC, Misra RDK. Biodegradable hydrogel-based biomaterials with high absorbent properties for non-adherent wound dressing. Int Wound J 2017;14:1076–87. https://doi.org/10.1111/iwj.12762.
[44] Wang C, Wu T, Liu G, Cheng R, Fei J, Song X, et al. Promoting coagulation and activating SMAD3 phosphorylation in wound healing via a dual-release thrombin-hydrogel. Chem Eng J 2020;397:125414. https://doi.org/10.1016/j.cej.2020.125414.
[45] Rosselle L, Cantelmo AR, Barras A, Skandrani N, Pastore M, Aydin D, et al. An 'on-demand' photothermal antibiotic release cryogel patch: evaluation of efficacy on an ex vivo model for skin wound infection. Biomater Sci 2020;8:5911–9. https://doi.org/10.1039/D0BM01535K.

[46] Madubuonu N, Aisida SO, Ali A, Ahmad I, Zhao T, Botha S, et al. Biosynthesis of iron oxide nanoparticles via a composite of Psidium guavaja-Moringa oleifera and their antibacterial and photocatalytic study. J Photochem Photobiol B Biol 2019;199:111601. https://doi.org/10.1016/j.jphotobiol.2019.111601.
[47] Rotman SG, Grijpma DW, Richards RG, Moriarty TF, Eglin D, Guillaume O. Drug delivery systems functionalized with bone mineral seeking agents for bone targeted therapeutics. J Contr Release 2018;269:88–99. https://doi.org/10.1016/j.jconrel.2017.11.009.
[48] Yu S, Wang S, Xie Z, Yu S, Li L, Xiao H, et al. Hyaluronic acid coating on the surface of curcumin-loaded ZIF-8 nanoparticles for improved breast cancer therapy: an in vitro and in vivo study. Colloids Surf B Biointerfaces 2021;203:111759.
[49] Manca ML, Manconi M, Meloni MC, Marongiu F, Allaw M, Usach I, et al. Nanotechnology for natural medicine: formulation of neem oil loaded phospholipid vesicles modified with argan oil as a strategy to protect the skin from oxidative stress and promote wound healing. Antioxidants 2021;10. https://doi.org/10.3390/antiox10050670.
[50] Alqahtani MS, Alqahtani A, Kazi M, Ahmad MZ, Alahmari A, Alsenaidy MA, et al. Wound-healing potential of curcumin loaded lignin nanoparticles. J Drug Deliv Sci Technol 2020;60:102020. https://doi.org/10.1016/j.jddst.2020.102020.
[51] Karaly AH, Sarhan WA, El-Sherbiny IM. Development of a silk fibroin-based multitask aerosolized nanopowder formula for efficient wound healing. Int J Biol Macromol 2021. https://doi.org/10.1016/j.ijbiomac.2021.03.178.
[52] Orlowski P, Zmigrodzka M, Tomaszewska E, Ranoszek-Soliwoda K, Czupryn M, Antos-Bielska M, et al. Tannic acid-modified silver nanoparticles for wound healing: the importance of size. Int J Nanomed 2018;13:991–1007. https://doi.org/10.2147/IJN.S154797.
[53] Belkacemi A, Laschke MW, Menger MD, Flockerzi V. Scratch migration assay and dorsal skinfold chamber for in vitro and in vivo analysis of wound healing. J Vis Exp 2019. https://doi.org/10.3791/59608.